Available online at website: https://journal.bcrec.id/index.php/bcrec

Bulletin of Chemical Reaction Engineering & Catalysis, 19 (2) 2024, 190-214

Research Article

Investigating the Structure of Defects in Heterometallic Zeolitic Imidazolate Frameworks ZIF-8(Zn/Cd) and Its Interaction with CO_2 Using First-Principle Calculations

Fajar Inggit Pambudi*, S. Sutarno, Adhi Dwi Hatmanto, Mita Patmawati, Tika Dwi Utari

Department of Chemistry, Faculty of Mathematics and Natural Sciences, Universitas Gadjah Mada, Sekip Utara Bulaksumur Yogyakarta 55281, Indonesia.

Received: 2nd March 2024; Revised: 28th March 2024; Accepted: 28th March 2024
Available online: 9th April 2024; Published regularly: August 2024

Abstract

Inducing defect in metal-organic frameworks (MOFs) is one of the strategies to modify the structure and properties of this functional material. Defect may occur in a pristine MOF due to missing organic linkers, metal centres and/or other structural behaviours. In this study, the structure of defects in multicomponent MOFs especially heterometallic MOFs of zeolitic imidazolate framework (ZIF-8(Zn/Cd)) was examined to unveil the possible preference defect formation due to missing 2-methylimidazolate (MeIm) and metal centres of Cd^{2+} and Zn^{2+}. Assuming defect formation due to the reaction between ZIF-8(Zn/Cd) and water, MeIm linker removal is energetically lower than removing metal centres of either Cd^{2+} or Zn^{2+}. But, the MeIm linker is easier to be removed when it is connected to Cd^{2+} (Cd-MeIm-Cd) than when it is connected to Zn^{2+} (Zn-MeIm-Zn). Defect in ZIF-8(Zn/Cd) affects the band gap energy to give slightly lower value than it in pristine ZIF-8(Zn/Cd). Non-covalent interaction (NCI) and interaction region indicator (IRI) analyses were also performed to indicate possible intermolecular forces such as van der Waals and attractive forces present in non-defective and defective ZIF-8(Zn/Cd). The presence of defects in mixed-metal ZIF-8(Zn/Cd) was also tested for its potential use on CO_2 adsorption. The interaction energy of CO_2 inside defective ZIF-8(Zn/Cd) indicates an exothermic behaviour where CO_2 molecule has a preference to be adsorbed inside the framework. This is especially when the capping agents at the defective ZIF-8(Zn/Cd) sites are removed to give open metal sites. This study provides insight how defects in multicomponent MOFs might presence affecting the structural and properties changes.

Keywords: zeolitic imidazolate frameworks; defects; DFT; carbon dioxide; doping; ZIF-8(Zn/Cd); ZIF

How to Cite: F.I. Pambudi, S. Sutarno, A.D. Hatmanto, M. Patmawati, T.D. Utari (2024). Investigating the Structure of Defects in Heterometallic Zeolitic Imidazolate Frameworks ZIF-8(Zn/Cd) and Its Interaction with CO_2 Using First-Principle Calculations. *Bulletin of Chemical Reaction Engineering & Catalysis*, 19 (1), 190-214 (doi: 10.9767/bcrec.20136)

Permalink/DOI: https://doi.org/10.9767/bcrec.20136
Supporting Information (SI): https://journal.bcrec.id/index.php/bcrec/article/downloadSuppFile/20136/5156

1. Introduction

Carbon capture technology is one of the crucial strategies to overcome the environmental thread due to the raising of CO_2 concentration in the atmosphere. One of the promising approaches is using functional materials which are effective and selective to capture CO_2 molecules. Several examples of functional materials for carbon capture are inorganic materials such as carbon-based materials, zeolite and zeo-type materials, metal oxide, hybrid inorganic and organic materials, etc. [1–5]. Further strategies to improve the affinity of functional materials are performed by inducing possible defect within the structure of functional materials [6,7].

Metal-organic frameworks (MOFs) possess an unprecedented diversity that can be fine-tuned to promote new functionalities. Both non-defective and defective MOFs may provide different properties and/or behaviour in response to the structural changes [8,9]. Many reports have

* Corresponding Author.
Email: fajar.inggit@ugm.ac.id (F.I. Pambudi)

shown that different kinds of defects may occur including missing linker, missing metal, and rotational defects within the structure [10,11]. Previous experimental works and computational studies concluded that defect structure can be identified within certain order of details and their impacts towards some applications [12–14]. Creating defect sites usually requires additional precursor during MOF synthesis such as modulator and mineralizer (acid or base) or through post-synthetic modification of the parent non-defective MOFs. In the latter case, the non-defective MOFs can be reacted or exposed to other chemicals that have probability to create defect by leaching the organic linkers or metal ions [15]. For example, defect in ZIF-8 can be created by exposing the crystal to water solvent [16]. In many studies, defects have been associated with the loss of some components of MOFs which may create an unbalanced charge within the structure. Therefore, capping agents are usually presence in the defect sites from the result of possible decomposition of solvent molecules or from modulators to promote a neutral charge [17,18].

Several examples of defects studies were conducted in UiO-66, ZIF-8, and MIL-53 [19–23]. In UiO-66, the defect structures due to missing linker and missing metals have been reported on their impact on the electronic properties. The presence of defect is predicted to change the electronic properties where the band gap is changing from the initial non-defective UiO-66 [24]. Another example is for ZIF-8 material, where the defect sites can be easily promoted by the presence of water. MIL-53(Fe) has also been studied in term of its defect and its impact toward photocatalytic activity [22]. In those studies, defect was studied on a MOF with single type of metal ions.

Tunability in MOFs structure provide an opportunity to make multicomponent MOFs where a single MOF structure may contain multi type of organic linker and/or different type of metal centres [25,26]. This modification has been reported to enhance several characteristic or properties of the initial MOFs [27]. Additionally, there is a possibility that the characteristic of a multicomponent MOFs can be further enhanced by incorporating defect within the structure. In our approach, we investigate the formation of defects and its effect in electronic properties for a multicomponent MOF, especially for heterometallic MOF. In this MOF type, the inorganic part of the structure consists of multiple type of metal centres which then coordinatively interact with the same organic linker to give a common framework structure. In defective heterometallic MOFs, there are several aspects that we want to investigate, such as: (1) The formation of defect due to missing organic linker and metal ions might be affected by the type of either metal centres or organic linkers; (2) The electronic properties of mixed-metal MOFs have been known to be different in some reports, therefore there is a possibility to further fine-tuned those properties by inducing defects in mixed-metal MOFs; (3) The presence of defects in mixed-metal MOFs may provide additional space in the structure which can be studied in term of intermolecular forces by using non-covalent interaction approach. Furthermore, the defect sites may provide additional binding sites for CO_2 molecule.

To understand defects in heterometallic MOFs, a zeolitic imidazolate framework (ZIF-8) has been chosen as the study case. ZIF-8 material consists of metal ions, such as: Zn^{2+}, Cd^{2+}, Co^{2+}, which interact with 2-methylimidazolate (MeIm) linker to form a 3-dimensional structure with cubic structure giving a sodalite topology (see Figure 1(a)) [28–30]. The metal ion is coordinated with four MeIm linkers to give a tetrahedral geometry mimicking the structure of $[SiO_4]_n$ in zeolite. The presence of mixed-metal in ZIF-8 and the impact into the structure have been reported, such as: ZIF-8(Zn/Cd) [31] and ZIF-8(Zn/Co) [28,32]. However, reports about defects in mixed-metal ZIF-8 are still scarce. In this study, the structural characteristic of non-defective and defective ZIF-8(Zn/Cd) is investigated to obtain an insight how defects due to water-induced reaction may occur and affect structural and electronic parameters. In addition, the potential use of the defective ZIF-8(Zn/Cd) was also tested for CO_2 adsorption.

2. Computational Methods

The structure of ZIF-8 has a cubic system with the lattice dimensions of $a = b = c = 18.1206$ Å and $a = b = c = 16.9910$ Å for ZIF-8(Cd) and ZIF-8(Zn), respectively [29,30]. However, to minimize the number of defect structures in ZIF-8, the structure was transformed to give a smaller representation of atom in non-orthorhombic primitive cell as shown in Figure 1(b) with the unit cell of $a = b = c = 15.6929$ Å and $\alpha = \beta = \gamma = 109.471°$ [33]. Starting from ZIF-8(Cd), mixed-metal ZIF-8(Zn/Cd) was constructed by replacing 3 Cd^{2+} ions with 3 Zn^{2+} ions to give Cd_3Zn_3-ZIF-8(Zn/Cd). Two possible configurations for ZIF-8(Zn/Cd) were chosen to give the location of either Cd^{2+} or Zn^{2+} with trimer (*T*) or disperse (*D*) structure. In *T* structure, the location of the same metal ions is adjacent to each other, while the location of the same metal ion type in *D* structure for example Cd^{2+} is alternating to Zn^{2+} ion (Figure S1a and S1b in the Supporting Information). The defect structure of both missing linker and missing metal ion were constructed from *T* and *D* structure accommodating different

crystallographic sites of either metal ion or MeIm linker. For example, in missing linker defect, there are 8 different structures annotated as 1DL, 2DL, 1TL, 2TL, 3TL, 4TL, 5TL and 6TL (*D* = disperse, *T* = trimer, *L* = missing linker) (see Figure S2-S5 in the Supporting Information). The 1DL and 2DL are differentiated from the removal of an MeIm linker which has two different crystallographic positions. The first is the MeIm in plane with the (111) lattice plane, while the second structure (2DL) is when MeIm linker is slightly tilting from the (111) lattice plane (see Figure S2 Supporting Information). The same is also applied for other TL structures. For missing metal defect structures, there are 6 structures annotated as 1DM, 2DM, 1TM, 2TM, 3TM, and 4TM (see Figure S6-S8 Supporting Information).

DFT calculations were performed with the Quickstep module implemented in the CP2K code [34]. All structures were optimized by relaxing both the atomic coordinates and the unit cell size while the angle between unit cell axis is kept fix. The calculation was performed using Perdew-Becke-Ernzerhof (PBE) with the addition of Grimme D3 correction to account for possible weak interactions [35,36]. The basis set of TZVP-MOLOPT was used for C, N, O, and H atoms while DZVP-MOLOPT was used for Cd and Zn. The Goedecker-Teter-Hutter (GTH) pseudopotential was used to treat the core electrons. An energy cutoff of 600 Ry was used in all calculations. The SCF convergence was set to 1×10^{-6} Hartree. The optimization was completed when the maximum force is less than 4.5×10^{-4} Ha.Bohr^{-1}. The contribution of spin effect was also checked for several configurations of both non-defective and defective structures. The results show no significant different for the electronic energy and

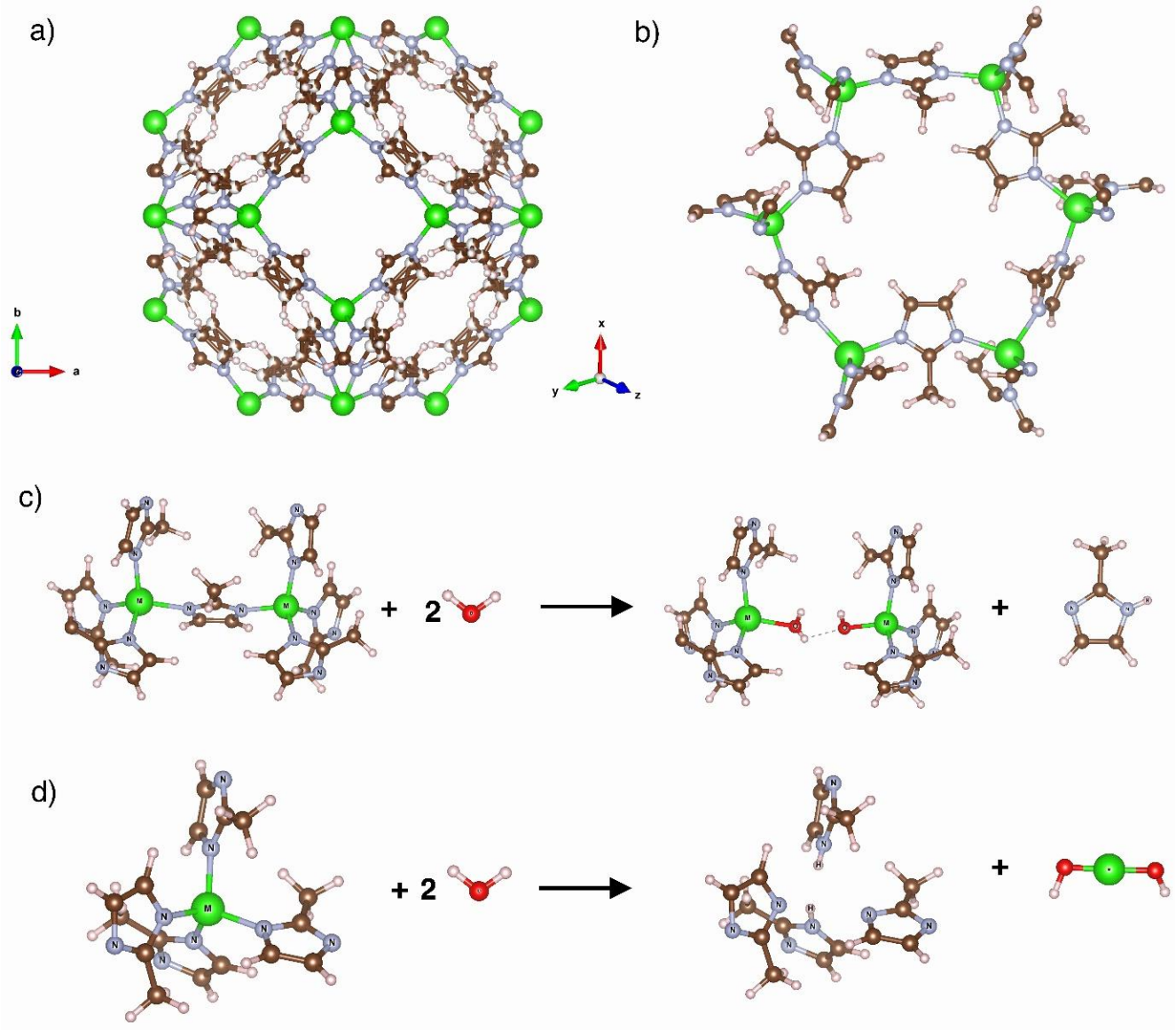

Figure 1. A cubic structure of ZIF-8 (a) and simplified non-orthorombic primitive cell of ZIF-8 (b). Reaction schemes for missing MeIm (c) and metal centre (d) are also given. M(metal), N, C, O, and H are coloured as green, cyan, red, and pink, respectively.

the band gap energy when DFT calculations were performed with spin effect and without the spin contribution. The electronic energy, band gap energy, and total DOS profile of DFT calculation with and without spin contribution are given in Table S1, Figure S9-S11 (Supporting Information).

Single point energy calculation was performed to obtain the reaction energy of defect formation. The reaction energy ($E_{reaction}$) for missing MeIm linker (Figure 1(c)) was calculated with the following equation (1):

$$E_{reaction} = \left(E_{defect} + E_{MeIm}\right) - \left(E_{MOF} - E_{water}\right) \quad (1)$$

E_{defect} is the defective energy of ZIF-8(Zn/Cd) due to missing MeIm, E_{MeIm} is energy of MeIm ligand, E_{MOF} is the energy of pristine ZIF-8(Zn/Cd) and E_{water} is energy of water molecule. The reaction energy for missing metal centre (Figure 1d) is calculated using the following equation (2):

$$E_{reaction} = \left(E_{defect} + E_{M(OH)_2}\right) - \left(E_{MOF} - E_{water}\right) \quad (2)$$

where, $E_{M(OH)2}$ is the energy of either $Zn(OH)_2$ or $Cd(OH)_2$.

Several selected structures of non-defective (T and D) and defective configuration were selected to unveil the structural behaviour through ab initio molecular dynamics (AIMD). The structural dynamics were studied with NVT at temperature of 298 K and 500 K. The time step was set to 0.5 fs. A Nose Hoover thermostat was used to control the temperature with a time constant of 50 fs. The trajectory files were stored to gain the atomic coordinates. The equilibrium phase was collected for the first 2.5 ps followed by the production phase for further 7.5 ps.

Selected defective structures of ZIF-8(Zn/Cd) were chosen to study the interaction with CO_2 molecule. A CO_2 molecule was located close to the defect sites of either missing linker or metal ion. Geometry optimization was performed with the same methods as calculating the defect structure through periodic DFT calculation. The energy of interaction between CO_2 and defective ZIF-8(Zn/Cd) was calculated as well as the charge density difference. Additionally, non-covalent interaction (NCI) and interaction region indicator (IRI) analyses were performed for selected structures to investigate possible interaction due to covalent bond or weak interaction [37].

3. Results and Discussion

3.1 Structure of Defective ZIF-8(Zn/Cd)

The presence of multi metals centres within ZIF-8 affect the structural parameters especially the lattice dimensions. In ZIF-8(Cd) and ZIF-8(Zn), the *a*-, *b*- and *c*- lattice dimensions are 15.837 Å and 14.842 Å in average, respectively. The change of the lattice dimension occurs when several metal centers in the parent ZIF-8 were replaced by different metal ion types to give mixed-metal ZIF-8(Zn/Cd). As seen in Figure S1 (Supporting Information), *D* and *T* represent mixed-metal ZIF-8 containing the same amount of Cd^{2+} and Zn^{2+} ions within the unit cell but differ in the arrangement to give a disperse and trimer structure, respectively. The unit cell is slightly lower than it in the initial ZIF-8(Cd) or higher than it in ZIF-8(Zn). In the *D* structure, the unit cell of *a*, *b* and *c* is 15.322, 15.335, and 15.318 Å, respectively, indicating approximately the same value along the axis. This is probably due to the alternate arrangement of Cd^{2+} and Zn^{2+} within the unit cell (see Figure S1 Supporting Information). However, when the location of Cd^{2+} and Zn^{2+} was changed to give a trimer configuration, the *b*-lattice diverges from *a*- and *c*-lattice as seen in Figure 2(a) and Table S2. The calculated unit cells of ZIF-8(Cd), ZIF-8(Zn), and ZIF-8(Zn/Cd) have been compared to the available experimental results as given in Table S3 of the Supporting Information [38]. The unit cell reduction from ZIF-8(Cd) to ZIF-8(Zn) is calculated to be 6.3% which is reasonably close with the reported experimental unit cell where the unit cell difference between ZIF-8(Cd) and ZIF-8(Zn) is 5.4%. In addition, the calculated unit cell of *D* and *T* structures has 3.2 to 3.3% difference relative to the unit cell of ZIF-8(Cd). This corresponds to the available experimental unit cell of ZIF-8(Zn/Cd) where the ratio between Zn^{2+} and Cd^{2+} is equal to give percent difference of 2.9% relative to the experimental unit cell of ZIF-8(Cd) (Table S3 Supporting Information).

Defective ZIF-8(Zn/Cd) due to missing linker also affect the lattice parameters. In 1DL to 6TL, the *a*-, *b*- and *c*-lattice parameters are diverging due to missing a linker in between of metal ions (Figure 2(a)). Although there is no indirect correlation between the size of each lattice parameter and the defect location, the volume is certainly lower than it in non-defective ZIF-8(Zn/Cd) structure. This is as expected since the organic linker is the backbone of ZIF-8 structure. Several reports show that missing linker may lead to deformation of MOF structure [39]. An example of diverse lattice parameters is given for 1TL structure where the position of missing linker is in between of *b*- and *c*-axes in the structure (see Figure S3 Supporting Information). The defect sites undergo arrangement during the geometry optimization which leads to the smaller unit cell dimension (15.093 Å in average) than the initial T structure (15.309 Å in average). The unit cell dimension is also affected when defect due to missing metal ions is present. Generally, the

structural changes are not rigorous as in missing linker given that the *a*-, *b*- and *c*- lattices are less diverging, and the volume is relatively higher than it in missing linker (Figure 2(a)).

The structural parameter such as the bond distance is observed both via static DFT and structural trajectory from the AIMD calculations at temperature of 298 K and 500 K. In Figure 2(b), it is shown that Cd−N distance is approximately the same in the entire range of defective ZIF-8(Zn/Cd) with an average bond distance of 2.228 Å. The same observation is also for Zn−N bond to give a length of 2.009 Å in average. From the AIMD trajectory at 298 K (Figure 2(c)), both Cd−N and Zn−N are still at around 2.2 Å and 2.0 Å, respectively for both non-defective and defective

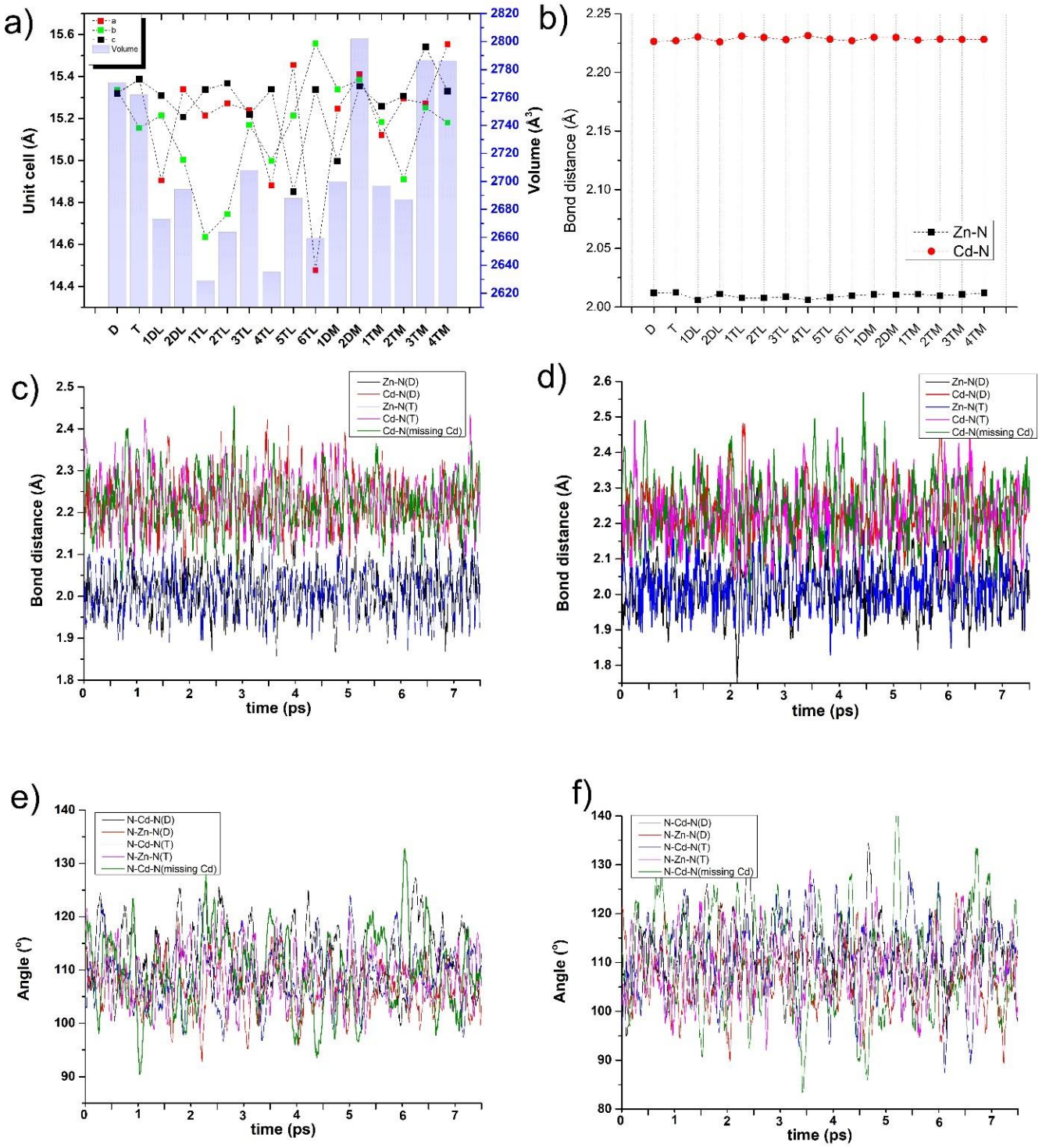

Figure 2. The lattice dimensions of defective mixed-metal ZIF-8(Zn/Cd) (a) and bond distance parameters in ZIF-8(Zn/Cd) from static DFT (b). Bond distance parameters of ZIF-8(Zn/Cd) from the AIMD trajectory are given in (c) and (d) at 298 K and 500 K, respectively. Angle parameters of N-M-N from AIMD trajectory is also shown in (e) and (f) at 298 K and 500 K, respectively.

ZIF-8(Zn/Cd). This indicates that the interaction between metal ions (Cd^{2+} or Zn^{2+}) and MeIm linkers is generally relative stable although defect is present.

The angle formed due to coordinative interaction between metal ions and ligand might provide insight why the unit cell of defective structure is diverging. From the AIMD calculation at 298 K shown in Figure 2(e), the N−Zn−N and N−Cd−N angle in missing metal ion is oscillating from 90.411° to 132.777° to maintain the tetrahedral geometry of $M(MeIm)_4$ structure. However, the averaged value of this angle is 109.403° showing the tetrahedral nature.

The AIMD calculation was also conducted at relatively higher temperature of 500 K as shown in Figure 2(d) and 2(f). The bond distance of Cd−N was averaged at 2.2 Å for non-defective and defective structures. This is the same as AIMD calculation at 298 K with average Cd−N distance of 2.2 Å. The bond distance of Zn−N is calculated to be 2.0 Å which is still the same with AIMD calculation at 298 K. This indicates that non-defective and defective ZIF-8(Zn/Cd) is predicted to be relatively stable at 500 K. The structure of ZIF-8 is reported experimentally to be stable at relatively high temperature. The structure is stable up to 350 °C under flowing air and 500 °C under nitrogen according to the thermal gravimetric analyses [40]. Another study also shows that the removal of guest molecules occurs between 100 °C to 200 °C and it remain stable until 425 °C under air flowing and 500 °C under nitrogen flow [41]. In our study, the AIMD trajectory predicts the stability of non-defective and defective structures.

The defect structure due to missing metal ion is occupied by two hydrogen atoms which are bonded to two neighbouring MeIm linkers. The structure is stabilized by the presence of hydrogen bonding between N−H and N atom from neighbouring MeIm as seen in Figure S12. The dynamics of hydrogen atom between two neighbouring imidazolate is examined through AIMD at temperatures of 298 K and 500 K as shown in Figure S12 (Supporting Information) indicating two possible average distances to nitrogen. The hydrogen is initially close to N1 with a distance of ~1.1 Å and moved away to a distance of ~1.6 Å, which is in close proximity to N2 with a distance of ~1.1 Å. In this case, the hydrogen is moving alternatingly in between two nitrogen atoms.

In missing MeIm defect, the linker is replaced by a water molecule attached to one end of metal ion and a hydroxide attached to the other end of metal ion. The distance of Zn−O or Cd−O is relatively similar to the distance of Zn−N or Cd−N, respectively. In various configuration of missing linker, the average Zn−O length is 2.005 Å which correlates to the Zn−N bond distance of 2.009 Å in non-defective ZIF-8(Zn/Cd). The same also occurs for Cd−O to give a bond distance of 2.232 Å which is the same as Cd−N in non-defective ZIF-8(Zn/Cd).

3.2 Energetic and Electronic Properties of Defective Mixed-metal ZIF-8(Zn/Cd)

The defect energy has been evaluated according to the reaction scheme shown in Figure 1. The energetic consideration might be used as a predictive tool for various defect structures from many possible configurations. In Figure 3, the energy of various defect structures was compared relative to the lowest energy state occurring for 1TL structure (highlighted with the green rectangular). The non-defective *D* and *T* structures have been compared in term of its relative stability. In this study, the ZIF-8(Zn/Cd) with *T* configuration is relatively more stable than

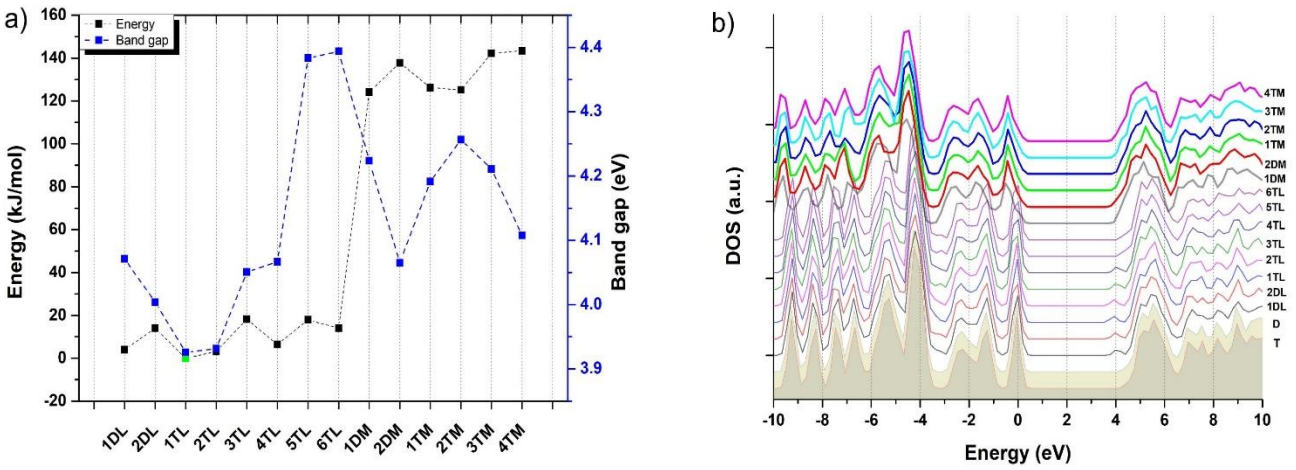

Figure 3. The energy and band gap of defective ZIF-8(Cd/Zn) are shown in (a) where the energy values are relative to the lowest energy configuration of 1TL shown with the green point. Total DOS of non-defective and defective are also given in (b).

D configuration with small energy difference (ΔE) of 0.01 eV between the two structures as shown in Table S4 in the Supporting Information. However, both *D* and *T* structures were used to generate possible defect structures due to missing metal ion or organic linker. The defect due to missing linker has relatively lower energy than it in the defect due to missing metal. The relative energy for missing linker defect is in the range of 0 kJ/mol to 18.19 kJ/mol, while the energy for missing metal defect is in the range of 124.13 kJ/mol to 143.41 kJ/mol. This behaviour can be explained due to the number of connectivity between metal ion and MeIm linker. In missing linker, a MeIm linker will be detached from two nearest metal ions and replaced by water and hydroxide. However, the number of connectivity in missing metal is higher which is four from coordination with four MeIm linkers.

Looking at the relative stability, a MeIm linker seem to be removed easily when it is adjacent to Cd^{2+} ion such as in 1TL and 2TL, where the MeIm is positioned in the middle (Cd−MeIm−Cd). However, when the missing MeIm is located in between of Zn^{2+} ion (Zn−MeIm−Zn), the relative energy is slightly higher such as in 5TL and 6TL. The same is also observed for missing metal. 1DM, 1TM, and 2TM are defect structure with missing Cd^{2+} ion having relative energies of 124.13 kJ/mol, 126.24 kJ/mol, and 125.12 kJ/mol, respectively. These energies are lower than defect due to missing Zn^{2+} ion in 2DM, 3TM, and 4TM structures with the energies of 137.81 kJ/mol, 142.16 kJ/mol, and 143.41 kJ/mol, respectively. The preference of defect formation can be associated with the structural behaviour especially the bond distance of Cd−N

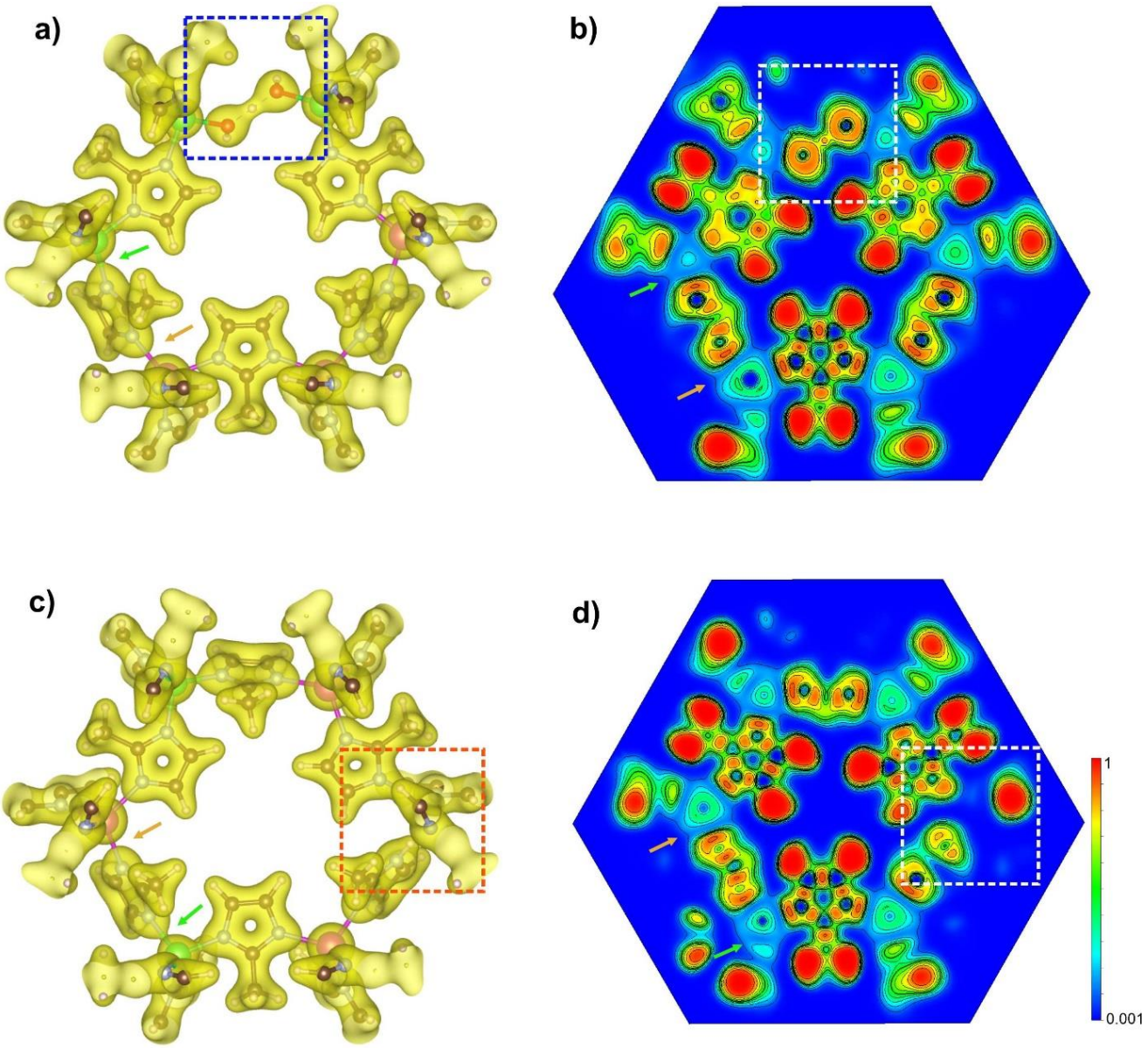

Figure 4. Electronic density of defect structure due to missing linker (a) and missing metal ion (c). Electron localization function (ELF) maps are also shown for missing linker (b) and missing metal ion (d) defect structure. An isosurface of 0.08 a.u. is applied for the electron density maps.

and Zn−N. The bond distance of Cd−N is relatively longer with 2.228 Å compared to it in Zn−N distance of 2.009 Å (Figure 2(b)). Therefore, the relative energy to remove Cd^{2+} ion is lower than removing Zn^{2+} ion. The same for removing MeIm linker attached to Cd^{2+} ion is relatively less energy than removing MeIm attached to Zn^{2+} ion.

The defects can be used also to fine tune the band gap energy which is beneficial for material with photo-induced applications. The band gap energy of mixed-metal ZIF-8(Zn/Cd) is slightly lower than bandgap energy of ZIF-8(Zn) with calculated bandgap value of 4.86 eV and experimental value of 4.96 eV [42]. Given in Figure 3(a), the band gap energy range is from 3.92 – 4.39 eV which is slightly lower than the non-defective ZIF-8(Zn/Cd) of *D* and *T* with 4.50 eV and 4.51 eV, respectively. Generally, the band gap energy is low when defect occurs due to missing metal ion and MeIm linker. The density of states (DOS) of various defect configuration provide insight into the electronic states present at the valence and conductance band. Non-defective *D* and *T* structure have electronic states around 0 eV (valence band) which is the same for the defect structure due to missing MeIm linker (Figure 3(b)). This electronic state is dominated by the *p* orbital of carbon and nitrogen atoms as shown in the partial DOS (see Figure S13-S14 Supporting Information). However, the electronic states at the valence band are slightly shifted toward negative energy for the structure with missing metal ion. In this case, the valence band is mostly dominated by *p* orbital (see also Figure S15 Supporting Information). Significant change of the electronic states occurs in the conductance band in which new electronic states emerge for the missing linker defect structures. This state is dominated by the presence of orbital *p* of N and C atoms according to the partial DOS (see Figure S16 Supporting Information). Different pattern is observed for missing metal ion structure, where the conductance band is slightly shifted toward lower energy with approximately the same pattern as occur in non-defective *D* and *T* structure. Generally, the electronic states shifted to lower energy where the highest peak of the valence band is slightly lower than the Fermi energy level (0 eV) indicating less metallic structure.

The electronic density of defective ZIF-8(Cd/Zn) provides further insight to explain the energetic trend of the defect structure. In Figure 4(a) and 4(c), the electronic density is examined at the same isosurface level of 0.08 a.u. It can be observed that the electron density is slightly overlap in the Zn-N bond as highlighted with the green arrow (see Figure 4(a) and 4(c)). However, the electronic distribution is slightly apart for Cd−N bond as shown with the light brown arrows. This might indicate that the interaction between Cd and N of MeIm is less stable than Zn−N. This is in relation with the defect energy in which the MeIm linker is easier to leave when it is connected to Cd^{2+} ion. The same also for missing metal ion, removing Cd^{2+} ion requires less energy than removing Zn^{2+} ion. Looking at the ELF maps (Figure 4(b) and 4(d)), it is shown a gap between Cd and N (light brown arrow) as well as for Zn and N (green arrow) indicating non-covalent nature which is more likely an ionic character. As comparison, the ELF maps for MeIm linker show an overlap indicating more covalent bond.

Looking at the missing MeIm structure (Figure 4(a)), the electronic density between Zn and O atom is slightly apart indicating possible weak coordinating behaviour. Interestingly, the hydrogen atom of water molecule interacts with hydroxyl group in a way that hydrogen is possibly to interchange in between two O atoms. This is confirmed by the ELF map, that there is still overlap region between H and two O atoms. The dissociation of OH bond from the capping H_2O molecule is possible since the water molecule is located in proximity to the capping −OH group attached to the next metal ions. The behaviour of H_2O molecule is visualised in Figure S17 (Supporting Information) for all structures. We

Table 1. The net atomic charge of selected atoms in defective ZIF-8(Zn/Cd) due to missing linker. Ht is hydrogen at terminal position, Hm is hydrogen of H_2O molecule close to −OH capping.

MOFs	Cd	Zn	Ht	Oa	Hm	Ob	Ht	Cd	Zn
1DL	0.827667	-	0.367279	-0.79014	0.388953	-0.78087	0.367299	-	0.736578
2DL	0.827415	-	0.366047	-0.79547	0.388785	-0.77852	0.364127	-	0.740137
1TL	0.830061	-	0.365083	-0.78571	0.380948	-0.79676	0.362522	0.827786	-
2TL	0.831853	-	0.364551	-0.79121	0.381885	-0.79689	0.363276	0.829179	-
3TL	0.834235	-	0.366164	-0.79491	0.398657	-0.79643	0.363542	-	0.739584
4TL	0.832878	-	0.367749	-0.79112	0.391547	-0.78229	0.367333	-	0.731534
5TL	-	0.738108	0.370265	-0.78263	0.399212	-0.78904	0.367808	-	0.743468
6TL	-	0.739747	0.366565	-0.77674	0.395898	-0.78324	0.369732	-	0.7361

have identified that the hydrogen atom from H_2O molecule is slightly distorted with O−H bond distance of 1.199 Å. This is slightly longer than typical O−H bond in H_2O of ~0.97 Å. This behaviour can be explained due to the hydrogen atom is relatively close to the more partial negative charge of oxygen from the −OH capping. To confirm the difference of the atomic charge, we have calculated net atomic charge based on the DDEC6 method as shown in Table 1. In Table 1, the order of the atom represents the relative position of atom in the crystal structure. The hydrogen atom is represented as Ht which is in terminal position without any significant influence from the adjacent oxygen atom, while Hm is originally hydrogen from the H_2O molecule that is in close proximity to the −OH group of the next metal ions. From Table 1, it is shown that the O atoms either from the H_2O molecule or the −OH group have negatively charge with an average charge of −0.78825*e*. The hydrogen located at the terminal (Ht) and in proximity to the −OH group (Hm) has slightly different charge. The Hm atom has an average charge of 0.390736*e* which is more positive than Ht with an average charge of 0.366209*e*. Therefore, we predict that the attraction of partial negative charge of O atoms affects the Hm atom. In missing metal defect, the metal ion is replaced by two hydrogen atoms attached to N atom of two MeIm linkers. The N−H bond can be identified to be more covalent in nature due to overlap in electronic density and ELF map (see Figure 4(d)).

3.3 Non-covalent Interaction (NCI) and Interaction Region Indicator (IRI)

The presence of defects in MOFs may provide new features, such as extra porosity, which leads to the addition of intermolecular forces that may presence in the structure. In non-defective mixed-metal ZIF-8(Zn/Cd), intermolecular forces such as weak van der Waals interaction are available occupying the space in between of MeIm linkers. This can be identified through non-covalent interaction analysis as given in Figure 5(a). The weak van der Waals is illustrated as the green isosurface (red arrow) indicating sign (λ,ρ) close to 0 a.u as seen in the reduced density gradient (RDG) curve and it dominates the intermolecular forces in non-defective ZIF-8(Zn/Cd). Several studies show that this type of intermolecular forces is most likely present in many other MOFs due to its nature as framework structure containing diverse types of organic linker.

The nature of coordination behaviour between metal ions (Cd^{2+} or Zn^{2+}) and MeIm linker also reveals through NCI analysis. Both non-defective and defective ZIF-8(Zn/Cd) contain relatively strong attractive force between metal ions and N of imidazolate as indicated by blue colour (red arrow) in Figure 5(b) and it presents approximately at $-0.08 <$ sign $(\lambda,\rho) < -0.05$ a.u. This attractive force is supporting the results from ELF and electron density map given in Figure 4. Following the ELF map, the bonding characteristic of metal ions and MeIm is probably more ionic character implying strong attractive force. However, the interaction strength may differ for Cd^{2+} and Zn^{2+} according to the electron density map.

Defects due to either missing linker or metal ion also show intermolecular forces at the defect sites. In Figure 5(c), missing metal ion defect gives extra van der Waals force due to the interaction between MeIm linkers. As previously mentioned, two hydrogen atoms are present to replace metal ion and connected to two MeIm linkers via N atom. These hydrogen atoms are stabilized by hydrogen bonding towards N atom of neighbour MeIm linker. This hydrogen bond can be identified with blue colour in the isosurface map as given with green arrow in the snippet of Figure 5(c). Hydrogen bond behaves as strong attractive force with $-0.08 <$ sign $(\lambda,\rho) < -0.05$ a.u in the RDG curve. In term of missing linker defect, water and hydroxide molecule interact through attractive forces with metal ions as indicated by the blue isosurface (Figure 5(d)) occupying the defect sites. This is in relation with the ELF maps, that the bonding character is likely ionic in nature. Additionally, one of the hydrogen atoms in water interact relatively strong with two oxygen from both the original water molecule and hydroxide as shown with the yellow arrow in Figure 5(d).

Additional analysis was performed using interaction region indicator (IRI). The IRI analysis can recognize where significant interactions such as covalent bond and weak interaction have formed. In Figure 5, the interaction mode is clearly identified whether the covalent bond or intermolecular interaction are present in the structures. The non-defective structure of *D* and *T* (Figure 5(a) and (b)) shows the covalent bond region domain which is mainly from the MeIm ligand as indicated by the blue isosurface. However, weak interactions are also present as indicated by the green isosurface. This is mainly from the intramolecular interaction between nearby MeIm ligands.

The IRI analysis of defective ZIF-8(Zn/Cd) due to missing metal ion and MeIm linker is given in Figure 5(c) and 5(d), respectively. A strong interaction in the form of covalent bond can be found from the MeIm ligand with the blue isosurface. However, the defect sites in missing metal ion (Figure 5(c)) is dominated by weak interaction in the form of possible van der Waals interaction. In missing MeIm defect, the weak interaction is also present in between nearby

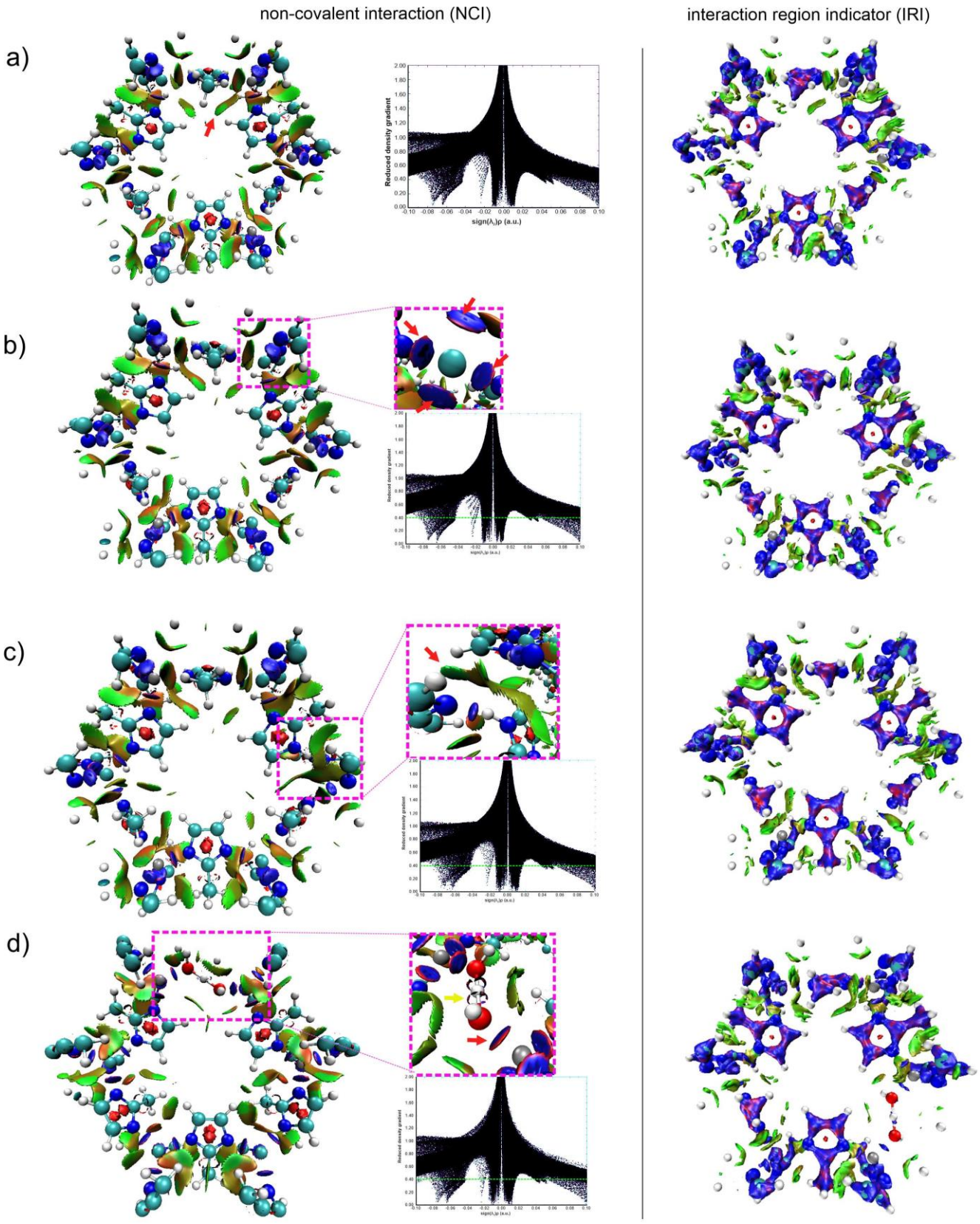

Figure 5. Noncovalent interaction maps (left) and interaction region indicator (IRI) analysis (right) showing possible location of intermolecular forces that might presence in non-defective structure of *D* (a) and *T* (b), and defect due to missing metal ion (c) and missing linker (d). Snippets of a structure section is also given for the NCI isosurface. Reduced density gradient (RDG) curves are given for each structure. Isosurface map was given with an isovalue of 0.4 a.u. for the NCI analysis and 0.8 a.u. for the IRI analysis.

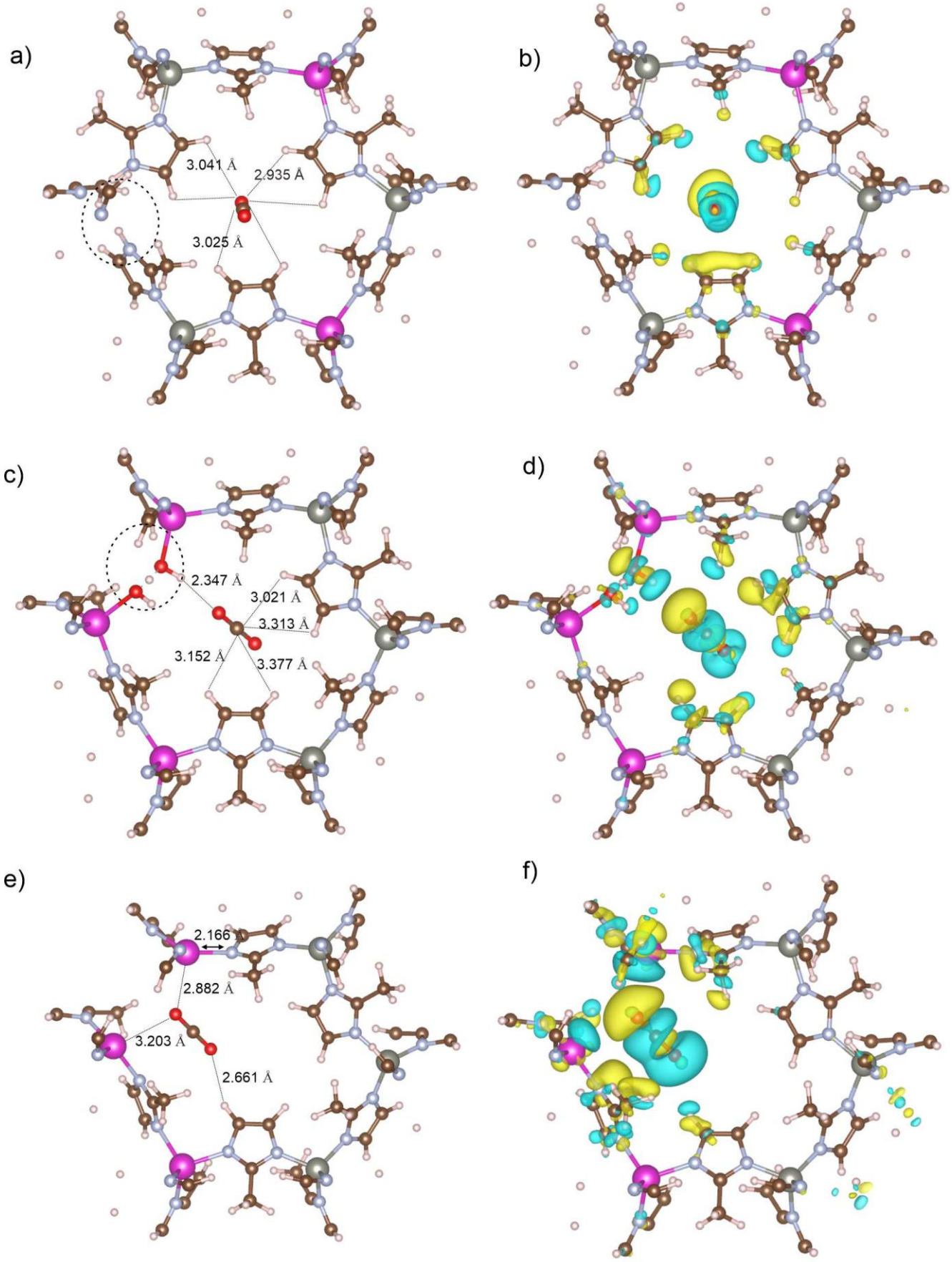

Figure 6. The optimized structure of defective ZIF-8(Zn/Cd) containing CO_2 with the electron density difference for 1DM (a,b), 1TL (c,d), and activated 1TL (e,f).

MeIm ligand. Since the metal ions are capped with H_2O and OH, the strong interaction is also observed in the defect sites. This IRI analysis confirm the non-covalent interaction (NCI) analysis and the electron density profile that the defect sites in mixed-metal ZIF-8(Zn/Cd) contain weak interaction to provide additional empty space for interaction with guest molecules such as CO_2 gas.

3.4 Interaction with CO_2

The use of multicomponent MOFs particularly mixed-metal MOFs has been reported in several studies. However, the adsorption of CO_2 in defective mixed-metal MOFs is still scarce. In this study, selected defective ZIF-8(Zn/Cd) structures have been tested for their interaction with CO_2. According to the energy profile in Figure 3, defective structures of 1TL and 1DM have the lowest relative energy than the other structures. These structures were selected for the interaction with CO_2. In Figure 6, the optimized structures of adsorbed CO_2 inside ZIF-8(Zn/Cd) are shown with the charge density profile. The adsorption energy shows that CO_2 inside 1DM has the lowest interaction energy of −26.2 kJ/mol, while CO_2 inside 1TL has interaction energy of −24.1 kJ/mol. This indicates that CO_2 has preferential to be adsorbed in defective ZIF-8(Zn/Cd) either missing linker or metal ions. Comparing the adsorption energy with pristine ZIF-8(Zn/Cd) shows small differences where CO_2 adsorbed in *D* and *T* has interaction energy of −23.9 kJ/mol and −24.3 kJ/mol, respectively. This value is relatively close to the reported value from DFT calculations of pristine ZIF-8(Zn) material with −20.96 kJ/mol (−5.01 kcal/mol) [43] and −24.6 kJ/mol [44].

The CO_2 molecule in the optimized structure is located approximately at the middle of the ZIF-8 pore (Figure 6(a,c)). In 1DM configuration, the CO_2 molecule resides approximately in the middle of the pore. Since a Cd^{2+} ion is missing in 1DM structure, the nature of the defect sites is still bulky due to the presence of four closest MeIm (see the black circle in Figure 6(a)). Therefore, CO_2 molecule might have less interaction with the defect sites in 1DM structure. The CO_2 molecule has the closest distance to MeIm linker at approximately 3 Å towards three MeIm around it. This results in less charge density difference compared to 1TL structure. In 1TL structure, the CO_2 molecule has the closest distance to the defect sites where H_2O and OH^- reside. CO_2 has a distance of 2.347 Å to the H of H_2O or OH^-, while the distance to the MeIm linkers is approximately 3 Å toward two closest MeIm linkers. The orientation of CO_2 molecule resulted in charge accumulation and depletion around the CO_2 and neighbouring MeIm linkers. In general, the presence of defect sites in mixed-metal ZIF-8(Zn/Cd) shows small differences in term of adsorption energy. This might occur due to the metal ion sites of either Cd^{2+} or Zn^{2+} are already occupied by the capping agent, therefore less open metal sites are available for additional binding sites of CO_2 molecules.

To confirm the adsorption energy of CO_2 in an activated structure, the capping agent of H_2O and OH^- in 1TL structure were removed and replaced with a CO_2 molecule as shown in Figure 6(e). When Cd^{2+} ions are more exposed to the CO_2 molecule, the adsorption energy of CO_2 decreases to −55.4 kJ/mol. This value is almost two times less than adsorption energy of CO_2 when the capping agents are still attached to the Cd^{2+} ions. Therefore, the presence of open metal sites in defective ZIF-8(Zn/Cd) is greatly reducing the adsorption energy compared to both pristine and defective ZIF-8(Zn/Cd) with the capping agents. The CO_2 molecule is located relatively close to both Cd^{2+} ions with a distance of 3.203 and 2.882 Å. In this configuration, CO_2 molecule also relatively close to the MeIm linker. This resulted in charge accumulation and depletion at the CO_2 and defective sites (Figure 6(f)).

4. Conclusion

Defects in heterometallic MOF of ZIF-8(Zn/Cd) have been thoroughly investigated with the help of first-principle calculations. The results show that defect due to missing MeIm linker has relatively lower energy than defect due to missing metal ions of either Zn^{2+} or Cd^{2+}. Furthermore, the MeIm linker is relatively easier to be removed when this linker is connected to the Cd^{2+} ion rather than to Zn^{2+} ion. For defect structures due to missing metal ions, the relative energy is lower when Cd^{2+} ion is missing from the structure than when Zn^{2+} ion is absence. This behaviour is confirmed by the electron density profile where the region of Cd−N has less electron density distribution than it in Zn−N bond. The presence of defect was also examined in term of non-covalent interaction and interaction region indicator. Missing MeIm and metal ions result in various intermolecular interactions such as a weaker van der Waals or stronger possible attractive interactions. In term of electronic properties, it is shown that missing linker or metal ions exhibits lower bandgap energy in the range of 3.92 – 4.39 eV than in pristine ZIF-8 (Zn/Cd). Additionally, the presence of defect in ZIF-8(Zn/Cd) was tested for its potential used on capturing CO_2 molecules. The presence of open metal sites in missing linker defect provides additional binding sites for CO_2 as indicated by the low adsorption energy. This study provides in-depth understanding on the nature of

defect structure in heterometallic MOFs where an organic linker has a preferential to be removed following the type of metal ions in its adjacent. An extra space or binding sites in defective heterometallic MOFs may be beneficial for application where host-guest system is dominant.

Acknowledgement

Authors thank to the support from Universitas Gadjah Mada through Academic Excellence Program Scheme B with a contract number of 7725/UN1.P.II/Dit-Lit/PT.01.03/2023.

CRedit Author Statement

Fajar Inggit Pambudi: Conceptualization, Methodology, Formal analysis, Writing – Original Draft, Supervision, Funding Acquisition; *Sutarno*: Supervision, Writing – Review and Editing; *Adhi Dwi Hatmanto*: Writing – Review and Editing, Formal analysis; *Mita Patmawati*: Investigation, Visualization, Formal analysis; *Tika Dwi Utari*: Investigation, Visualization, Formal analysis

Conflict of Interest

On behalf of all authors, the corresponding author states that there is no conflict of interest.

References

[1] Zhang, S., Zheng, M., Tang, Y., Zang, R., Zhang, X., Huang, X., Chen, Y., Yamauchi, Y., Kaskel, S., Pang, H. (2022). Understanding Synthesis–Structure–Performance Correlations of Nanoarchitectured Activated Carbons for Electrochemical Applications and Carbon Capture. *Advanced Functional Materials*, 32(40), 2204714. DOI: 10.1002/adfm.202204714

[2] Sun, H., Zhang, Y., Guan, S., Huang, J., Wu, C. (2020). Direct and highly selective conversion of captured CO_2 into methane through integrated carbon capture and utilization over dual functional materials. *Journal of CO_2 Utilization*, 38, 262–272. DOI: 10.1016/j.jcou.2020.02.001

[3] Glenna, D.M., Jana, A., Xu, Q., Wang, Y., Meng, Y., Yang, Y., Neupane, M., Wang, L., Zhao, H., Qian, J., Snyder, S.W. (2023). Carbon Capture: Theoretical Guidelines for Activated Carbon-Based CO_2 Adsorption Material Evaluation. *The Journal of Physical Chemistry Letters*, 14(47), 10693–10699. DOI: 10.1021/acs.jpclett.3c02711

[4] Chatterjee, S., Jeevanandham, S., Mukherjee, M., Vo, D.-V.N., Mishra, V. (2021). Significance of re-engineered zeolites in climate mitigation – A review for carbon capture and separation. *Journal of Environmental Chemical Engineering*, 9(5), 105957. DOI: 10.1016/j.jece.2021.105957

[5] Aniruddha, R., Sreedhar, I., Reddy, B.M. (2020). MOFs in carbon capture-past, present and future. *Journal of CO_2 Utilization*, 42, 101297. DOI: 10.1016/j.jcou.2020.101297

[6] Jelmy, E.J., Thomas, N., Mathew, D.T., Louis, J., Padmanabhan, N.T., Kumaravel, V., John, H., Pillai, S.C. (2021). Impact of structure, doping and defect-engineering in 2D materials on CO_2 capture and conversion. *Reaction Chemistry & Engineering*, 6 (10), 1701–1738. DOI: 10.1039/D1RE00214G

[7] Li, Y., Liu, L., Yu, H., Zhao, Y., Dai, J., Zhong, Y., Pan, Z., Yu, H. (2022). Synergy of developed micropores and electronic structure defects in carbon-doped boron nitride for CO_2 capture. *Science of The Total Environment*, 811, 151384. DOI: 10.1016/j.scitotenv.2021.151384

[8] Fang, Z., Bueken, B., De Vos, D.E., Fischer, R.A. (2015). Defect-Engineered Metal-Organic Frameworks. *Angewandte Chemie - International Edition*, 54(25), 7234–7254. DOI: 10.1002/anie.201411540

[9] Dissegna, S., Epp, K., Heinz, W.R., Kieslich, G., Fischer, R.A. (2018). Defective Metal-Organic Frameworks. *Advanced Materials*, 30(37), 1704501. DOI: 10.1002/ADMA.201704501

[10] Pambudi, F.I., Anderson, M.W., Attfield, M.P. (2019). Unveiling the mechanism of lattice-mismatched crystal growth of a core–shell metal–organic framework. *Chemical Science*, 10(41), 9571–9575. DOI: 10.1039/C9SC03131F

[11] Pambudi, F.I., Anderson, M.W., Attfield, M.P. (2021). Crystal growth of the core and rotated epitaxial shell of a heterometallic metal–organic framework revealed with atomic force microscopy. *Faraday Discussions*, 231, 112–126. DOI: 10.1039/D1FD00033K

[12] Xiang, W., Zhang, Y., Chen, Y., Liu, C.J., Tu, X. (2020). Synthesis, characterization and application of defective metal-organic frameworks: Current status and perspectives. *Journal of Materials Chemistry A*, 8(41), 21526–21546. DOI: 10.1039/d0ta08009h

[13] Wu, Y., Duan, H., Xi, H. (2020). Machine Learning-Driven Insights into Defects of Zirconium Metal–Organic Frameworks for Enhanced Ethane–Ethylene Separation. *Chemistry of Materials*, 32(7), 2986–2997. DOI: 10.1021/acs.chemmater.9b05322

[14] Liu, L., Chen, Z., Wang, J., Zhang, D., Zhu, Y., Ling, S., Huang, K.W., Belmabkhout, Y., Adil, K., Zhang, Y., Slater, B., Eddaoudi, M., Han, Y. (2019). Imaging defects and their evolution in a metal–organic framework at sub-unit-cell resolution. *Nature Chemistry*, 11(7), 622–628. DOI: 10.1038/s41557-019-0263-4

[15] Mandal, S., Natarajan, S., Mani, P., Pankajakshan, A. (2021). Post-Synthetic Modification of Metal–Organic Frameworks Toward Applications. *Advanced Functional Materials*, 31(4), 2006291. DOI: 10.1002/ADFM.202006291

[16] Zhang, C., Han, C., Sholl, D. S., Schmidt, J. R. (2016). Computational Characterization of Defects in Metal-Organic Frameworks: Spontaneous and Water-Induced Point Defects in ZIF-8. *Journal of Physical Chemistry Letters*, *7*(3), 459–464. DOI: 10.1021/acs.jpclett.5b02683

[17] Fast, C.D., Woods, J., Lentchner, J., Makal, T.A. (2019). Stabilizing defects in metal–organic frameworks: pendant Lewis basic sites as capping agents in UiO-66-type MOFs toward highly stable and defective porous materials. *Dalton Transactions*, 48(39), 14696–14704. DOI: 10.1039/C9DT03004B

[18] Mileo, P.G.M., Cho, K.H., Chang, J.S., Maurin, G. (2021). Water adsorption fingerprinting of structural defects/capping functions in Zr–fumarate MOFs: a hybrid computational-experimental approach. *Dalton Transactions*, 50(4), 1324–1333. DOI: 10.1039/D0DT03705B

[19] Bristow, J.K., Svane, K.L., Tiana, D., Skelton, J.M., Gale, J.D., Walsh, A. (2016). Free energy of ligand removal in the metal-organic framework UiO-66. *Journal of Physical Chemistry C*, 120 (17), 9276–9281. DOI: 10.1021/acs.jpcc.6b01659

[20] Tan, K., Pandey, H., Wang, H., Velasco, E., Wang, K.Y., Zhou, H.C., Li, J., Thonhauser, T. (2021). Defect Termination in the UiO-66 Family of Metal-Organic Frameworks: The Role of Water and Modulator. *Journal of the American Chemical Society*, 143(17), 6328–6332. DOI: 10.1021/jacs.1c01408

[21] Chaemchuen, S., Luo, Z., Zhou, K., Mousavi, B., Phatanasri, S., Jaroniec, M., Verpoort, F. (2017). Defect formation in metal–organic frameworks initiated by the crystal growth-rate and effect on catalytic performance. *Journal of Catalysis*, 354, 84–91. DOI: 10.1016/j.jcat.2017.08.012

[22] Jiang, D., Zhu, Y., Chen, M., Huang, B., Zeng, G., Huang, D., Song, B., Qin, L., Wang, H., Wei, W. (2019). Modified crystal structure and improved photocatalytic activity of MIL-53 via inorganic acid modulator. *Applied Catalysis B: Environmental*, 255, 117746. DOI: 10.1016/j.apcatb.2019.117746

[23] Cheng, P., Hu, Y.H. (2016). Acetylene adsorption on defected MIL-53. *International Journal of Energy Research*, 40 (6), 846–852. DOI: 10.1002/ER.3492

[24] Svane, K.L., Bristow, J.K., Gale, J.D., Walsh, A. (2018). Vacancy defect configurations in the metal–organic framework UiO-66: energetics and electronic structure. *Journal of Materials Chemistry A*, 6 (18), 8507–8513. DOI: 10.1039/C7TA11155J

[25] Abednatanzi, S., Gohari Derakhshandeh, P., Depauw, H., Coudert, F.X., Vrielinck, H., Van Der Voort, P., Leus, K. (2019). Mixed-metal metal-organic frameworks. *Chemical Society Reviews*, 48, 2535–2565. DOI: 10.1039/c8cs00337h

[26] Denny, M.S., Kalaj, M., Bentz, K.C., Cohen, S.M. (2018). Multicomponent metal-organic framework membranes for advanced functional composites. *Chemical Science*, 9(47), 8842–8849. DOI: 10.1039/c8sc02356e

[27] Sun, D., Sun, F., Deng, X., Li, Z. (2015). Mixed-Metal Strategy on Metal-Organic Frameworks (MOFs) for Functionalities Expansion: Co Substitution Induces Aerobic Oxidation of Cyclohexene over Inactive Ni-MOF-74. *Inorganic Chemistry*, 54(17), 8639–8643. DOI: 10.1021/acs.inorgchem.5b01278

[28] Zhou, K., Mousavi, B., Luo, Z., Phatanasri, S., Chaemchuen, S., Verpoort, F. (2017). Characterization and properties of Zn/Co zeolitic imidazolate frameworks vs. ZIF-8 and ZIF-67. *Journal of Materials Chemistry A*, 5(3), 952–957. DOI: 10.1039/C6TA07860E

[29] Park, K.S., Ni, Z., Côté, A.P., Choi, J.Y., Huang, R., Uribe-Romo, F.J., Chae, H.K., O'Keeffe, M., Yaghi, O.M. (2006). Exceptional chemical and thermal stability of zeolitic imidazolate frameworks. *Proceedings of the National Academy of Sciences of the United States of America*, 103 (27), 10186–10191. DOI: 10.1073/pnas.0602439103

[30] Tian, Y.Q., Yao, S.Y., Gu, D., Cui, K.H., Guo, D.W., Zhang, G., Chen, Z.X., Zhao, D.Y. (2010). Cadmium imidazolate frameworks with polymorphism, high thermal stability, and a large surface area. *Chemistry - A European Journal*, 16 (4), 1137–1141. DOI: 10.1002/chem.200902729

[31] Sun, J., Semenchenko, L., Lim, W.T., Ballesteros Rivas, M.F., Varela-Guerrero, V., Jeong, H.K. (2018). Facile synthesis of Cd-substituted zeolitic-imidazolate framework Cd-ZIF-8 and mixed-metal CdZn-ZIF-8. *Microporous and Mesoporous Materials*, 264, 35–42. DOI: 10.1016/j.micromeso.2017.12.032

[32] Zaręba, J.K., Nyk, M., Samoć, M. (2016). Co/ZIF-8 Heterometallic Nanoparticles: Control of Nanocrystal Size and Properties by a Mixed-Metal Approach. *Crystal Growth & Design*, 16 (11), 6419–6425. DOI: 10.1021/acs.cgd.6b01090

[33] Chung, Y.G., Haldoupis, E., Bucior, B.J., Haranczyk, M., Lee, S., Zhang, H., Vogiatzis, K.D., Milisavljevic, M., Ling, S., Camp, J.S., Slater, B., Siepmann, J.I., Sholl, D.S., Snurr, R.Q. (2019). Advances, Updates, and Analytics for the Computation-Ready, Experimental Metal–Organic Framework Database: CoRE MOF 2019. *Journal of Chemical & Engineering Data*, 64 (12), 5985–5998. DOI: 10.1021/acs.jced.9b00835

[34] Kühne, T.D., Iannuzzi, M., Del Ben, M., Rybkin, V.V., Seewald, P., Stein, F., Laino, T., Khaliullin, R.Z., Schütt, O., Schiffmann, F., Golze, D., Wilhelm, J., Chulkov, S., Bani-Hashemian, M.H., Weber, V., *et al*. (2020). CP2K: An electronic structure and molecular dynamics software package - Quickstep: Efficient and accurate electronic structure calculations. *The Journal of Chemical Physics*, 152(19), 194103. DOI: 10.1063/5.0007045

[35] Perdew, J.P., Burke, K., Ernzerhof, M. (1996). Generalized gradient approximation made simple. *Physical Review Letters*, 77(18), 3865–3868. DOI: 10.1103/PhysRevLett.77.3865

[36] Grimme, S., Antony, J., Ehrlich, S., Krieg, H. (2010). A consistent and accurate ab initio parametrization of density functional dispersion correction (DFT-D) for the 94 elements H-Pu. *Journal of Chemical Physics*, 132(15), 134101. DOI: 10.1063/1.3382344

[37] Lu, T., Chen, Q. (2021). Interaction Region Indicator: A Simple Real Space Function Clearly Revealing Both Chemical Bonds and Weak Interactions. *Chemistry–Methods*, 1(5), 231–239. DOI: 10.1002/cmtd.202100007

[38] Sapnik, A.F., Geddes, H.S., Reynolds, E.M., Yeung, H.H.-M., Goodwin, A.L. (2018). Compositional inhomogeneity and tuneable thermal expansion in mixed-metal ZIF-8 analogues. *Chemical Communications*, 54(69), 9651–9654. DOI: 10.1039/C8CC04172E

[39] Zheng, B., Fu, F., Wang, L.L., Wang, J., Du, L., & Du, H. (2018). Effect of Defects on the Mechanical Deformation Mechanisms of Metal-Organic Framework-5: A Molecular Dynamics Investigation. *Journal of Physical Chemistry C*, 122 (8), 4300–4306. DOI: 10.1021/ACS.JPCC.7B10928

[40] Yin, H., Kim, H., Choi, J., Yip, A.C.K. (2015). Thermal stability of ZIF-8 under oxidative and inert environments: A practical perspective on using ZIF-8 as a catalyst support. *Chemical Engineering Journal*, 278, 293–300. DOI: 10.1016/j.cej.2014.08.075

[41] James, J.B., Lin, Y.S. (2016). Kinetics of ZIF-8 Thermal Decomposition in Inert, Oxidizing, and Reducing Environments. *The Journal of Physical Chemistry C*, 120(26), 14015–14026. DOI: 10.1021/acs.jpcc.6b01208

[42] Yang, X., Qiu, L., Luo, X. (2018). ZIF-8 derived Ag-doped ZnO photocatalyst with enhanced photocatalytic activity. *RSC Advances*, 8(9), 4890–4894. DOI: 10.1039/C7RA13351K

[43] Paudel, H.P., Shi, W., Hopkinson, D., Steckel, J.A., Duan, Y. (2021). Computational modelling of adsorption and diffusion properties of CO_2 and CH_4 in ZIF-8 for gas separation applications: a density functional theory approach. *Reaction Chemistry & Engineering*, 6(6), 990–1001. DOI: 10.1039/D0RE00416B

[44] Fischer, M., Bell, R.G. (2014). Interaction of hydrogen and carbon dioxide with sod-type zeolitic imidazolate frameworks: A periodic DFT-D study. *CrystEngComm*, 16(10), 1934–1949. DOI: 10.1039/c3ce42209g